The GOME-2 total column ozone product: Retrieval algorithm and ground-based validation

D. G. Loyola,[1] M. E. Koukouli,[2] P. Valks,[1] D. S. Balis,[2] N. Hao,[1] M. Van Roozendael,[3] R. J. D. Spurr,[4] W. Zimmer,[1] S. Kiemle,[1] C. Lerot,[3] and J.-C. Lambert[3]

Received 25 June 2010; revised 11 January 2011; accepted 24 January 2011; published 5 April 2011.

[1] The Global Ozone Monitoring Instrument (GOME-2) was launched on EUMESAT's MetOp-A satellite in October 2006. This paper is concerned with the retrieval algorithm GOME Data Processor (GDP) version 4.4 used by the EUMETSAT Satellite Application Facility on Ozone and Atmospheric Chemistry Monitoring (O3M-SAF) for the operational generation of GOME-2 total ozone products. GDP 4.4 is the latest version of the GDP 4.0 algorithm, which is employed for the generation of official Level 2 total ozone and other trace gas products from GOME and SCIAMACHY. Here we focus on enhancements introduced in GDP 4.4: improved cloud retrieval algorithms including detection of Sun glint effects, a correction for intracloud ozone, better treatment of snow and ice conditions, accurate radiative transfer modeling for large viewing angles, and elimination of scan angle dependencies inherited from Level 1 radiances. Furthermore, the first global validation results for 3 years (2007–2009) of GOME-2/MetOp-A total ozone measurements using Brewer and Dobson measurements as references are presented. The GOME-2/MetOp-A total ozone data obtained with GDP 4.4 slightly underestimates ground-based ozone by about 0.5% to 1% over the middle latitudes of the Northern Hemisphere and slightly overestimates by around 0.5% over the middle latitudes in the Southern Hemisphere. Over high latitudes in the Northern Hemisphere, GOME-2 total ozone has almost no offset relative to Dobson readings, while over high latitudes in the Southern Hemisphere GOME-2 exhibits a small negative bias below 1%. For tropical latitudes, GOME-2 measures on average lower ozone by 0% to 2% compared to Dobson measurements.

Citation: Loyola, D. G., et al. (2011), The GOME-2 total column ozone product: Retrieval algorithm and ground-based validation, *J. Geophys. Res.*, *116*, D07302, doi:10.1029/2010JD014675.

1. Introduction

[2] Long-term satellite total ozone data sets of high accuracy and stability are essential for atmospheric monitoring; this is even more important following the 1987 Montreal Protocol and its subsequent amendments [e.g., *Zerefos et al.*, 2009]. The Global Ozone Monitoring Experiment–2 (GOME-2) is one of the new-generation European instruments carried onboard the EUMETSAT MetOp-A satellite launched in October 2006. It continues the long-term monitoring of atmospheric trace gases started by GOME (launched on ESA ERS-2 platform in 1995) [*Burrows et al.*, 1999] and continued with SCIAMACHY (launched on ESA ENVISAT platform in 2002) [*Bovensmann et al.*, 1999]. GOME data based on version 4.0 of the GOME Data Processor (GDP 4.0 [*Van Roozendael et al.*, 2006]) have been validated and compared with ground-based and TOMS satellite data [*Balis et al.*, 2007a], showing remarkable stability of 0.10%/decade and an agreement within 1% relative to the ground-based correlative measurements. SCIAMACHY data have been recently reprocessed with GDP 4.0 and compared with other satellite measurements [*Lerot et al.*, 2009], showing an agreement within 2% and a drift of −0.5%/year in the ozone columns. This record is currently being used in a number of operational and scientific applications, including long-term trend analysis [*Loyola et al.*, 2009]. Two more GOME-2 sensors on the MetOp-B and MetOp-C platforms will extend the GOME-type data record until 2020 covering an expected time span of at least 25 years. This unique data record will be further extended by the Sentinel-5 precursor to be launched by the middle of this decade, and the Sentinel-4 and Sentinel-5 sensors to be launched by the end of this decade.

[3] GOME-2 is a nadir-viewing scanning spectrometer with a ground pixel size of 80 × 40 km^2 and a scan width of 1920 km that provides an almost daily global coverage. GOME-2 covers the same spectral range as GOME, i.e.,

[1]German Aerospace Center, Wessling, Germany.
[2]Laboratory of Atmospheric Physics, Aristotle University of Thessaloniki, Thessaloniki, Greece.
[3]Belgian Institute for Space Aeronomy, Brussels, Belgium.
[4]RT Solutions, Inc., Cambridge, Massachusetts, USA.

0148-0227/11/2010JD014675

from 240 to 790 nm, with spectral resolution varying from 0.26 to 0.51 nm. Additionally, two polarization components are measured at 30 broadband channels covering the full spectral range. The MetOp-A satellite follows a Sun-synchronous orbit with a mean altitude of 817 km. The overpass local time at the equator is 0930 LT with a repeat cycle of 29 days. For more details, see *Munro et al.* [2006].

[4] Operational GOME-2 Level 1 products are generated at EUMETSAT headquarters in Darmstadt, Germany and are broadcasted via the EUMETCast system in data chunks each containing 3 min of measurements. EUMETSAT O3M-SAF is responsible for processing, archiving, validating and disseminating atmospheric composition products such as trace gases O_3, NO_2, SO_2, BrO, H_2O, HCHO, and OClO, as well as aerosols, cloud properties and surface ultraviolet radiation from GOME-2.

[5] The GOME-2 Level 1 products are received at the O3M-SAF processing facility in DLR, Germany 1 h and 45 min after sensing. The DLR multimission payload ground segment system [*Heinen et al.*, 2009] controls the reception, processing, archiving, ordering and dissemination of the GOME-2 total column and cloud products. The GOME-2 Level 1 products are processed with the UPAS (Universal Processor for UV/VIS Atmospheric Spectrometers) system and the resulting GOME-2 Level 2 products are disseminated through EUMETCast, WMO/GTS and the Internet. The Level 1 data reception, processing with UPAS and Level 2 data dissemination takes less than 15 min in total. The end user receives the GOME-2 Level 2 near-real-time total column products in less than 2 h after sensing with a committed highly reliable service of 24 h a day, 365 days a year. DLR provides also offline and reprocessed GOME-2 Level 2 consolidate products on an orbital basis. These can be ordered via the EUMETSAT Data Centre Information (http://archive.eumetsat.int/umarf/) and DLR EOWEB systems (http://eoweb.dlr.de).

[6] In the following, the improved GDP 4.4 algorithm used for reprocessing the 4 year GOME-2 total ozone record is described in detail. Subsequently, the GOME-2 total ozone data are validated against the same ground-based Brewer and Dobson data used for the GOME validation in order to check the consistency of these new satellite data with the existing long-term total ozone records.

2. GDP 4.4 Algorithm

[7] The algorithm GOME Data Processor (GDP) version 4.4 is integrated into the Universal Processor for Atmospheric Spectrometers (UPAS) processing system that generates operational GOME-2 total ozone products. GDP 4.4 is the latest incarnation of the GDP 4.0 algorithm [*Van Roozendael et al.*, 2006]. The algorithm employs the two-step Differential Optical Absorption Spectroscopy (DOAS) method, with slant column fitting followed by Air Mass Factor (AMF) conversion to the vertical column density. The slant column fitting is based on Beer's law for trace gas absorption, and includes a polynomial closure term to deal with broadband signatures over the 325–335 nm fitting window. The fitting includes amplitudes for the effective temperature of the ozone absorption,NO_2 absorption and for spectral interference signatures (instrumental undersampling, ring effect filling in of solar Fraunhofer features), and a provision for earthshine/solar spectra wavelength registration offsets. Undersampling correction [*Slijkhuis et al.*, 1999] normally used by GOME-1 and SCIAMACHY is not needed because GOME-2 oversamples by a factor 2. In the retrieval, the use of reconvolved GOME-FM98 ozone cross sections [*Burrows et al.*, 1999], with a preshift of +0.016 nm and correction for the so-called I_0 effect, provides the most consistent and stable results for GOME-2.

[8] AMFs are calculated online with the multiple-scattering radiative transfer code LIDORT [*Spurr*, 2008]. Optical property setups for the AMF computations are based on the TOMS v8 ozone profile climatology classified by total column [*Bhartia et al.*, 2002; *McPeters et al.*, 2007], and the assumption of a Rayleigh scattering atmosphere. Scattering by aerosols is implicitly treated through the cloud correction scheme (section 2.1). AMFs are computed at a single wavelength of 325.5 nm [*Van Roozendael et al.*, 2006]. The vertical column V and the AMFs are adjusted iteratively to reflect the DOAS slant column result using the relation:

$$V^{(n+1)} = \frac{\frac{E}{M^{(n)}} + \Phi G^{(n)} A^{(n)}_{cloud}}{(1-\Phi)A^{(n)}_{clear} + \Phi A^{(n)}_{cloud}} \quad (1)$$

where the superscript (n) indicates the iteration number, E is the DOAS-retrieved slant column, M is the molecular Ring correction, A_{clear} the clear sky AMF, A_{cloud} the AMF for the atmosphere down to the cloud top level, the "ghost column" G is the quantity of ozone below the cloud top height and Φ is the intensity-weighted cloud fraction. This relation assumes the independent pixel approximation (IPA) for partially cloudy and cloud-filled scenes. The iteration stops after the relative change in V falls below a suitably small convergence criterion (0.1% is used in practice); convergence is rapid in the vast majority of cases (2–4 iterations).

[9] GDP 4.0 includes a molecular Ring correction M, dependent on the total AMF [*Van Roozendael et al.*, 2006], that is applied to the slant column to deal with distortion of ozone absorption features due to inelastic rotational Raman scattering effects. In the IPA, clouds are treated as Lambertian reflecting surfaces, with cloud properties retrieved from GOME-2 measurements using the OCRA (cloud fraction) and ROCINN (cloud top pressure and albedo) algorithms [*Loyola et al.*, 2007].

[10] The algorithm enhancements introduced in GDP 4.4 compared with GDP 4.0 are described in sections 2.1–2.5.

2.1. Improved Cloud Retrieval Algorithms

[11] GOME-2 footprints with 80 × 40 km^2 are comparatively large and therefore the retrieval is often affected by cloud-contaminated scenes. Three cloud properties (cloud fraction, cloud top height and cloud top albedo) are needed for computing the various entries in equation (1). In GDP 4.0 we use the OCRA and ROCINN algorithms [*Loyola et al.*, 2007] for obtaining GOME-2 cloud information: OCRA provides the cloud fraction using the broadband polarization measurements, and ROCINN provides cloud top height and cloud top albedo from measurements in and adjacent to the oxygen A band around 760 nm. Note that being sensitive to light scattering by clouds, OCRA is also

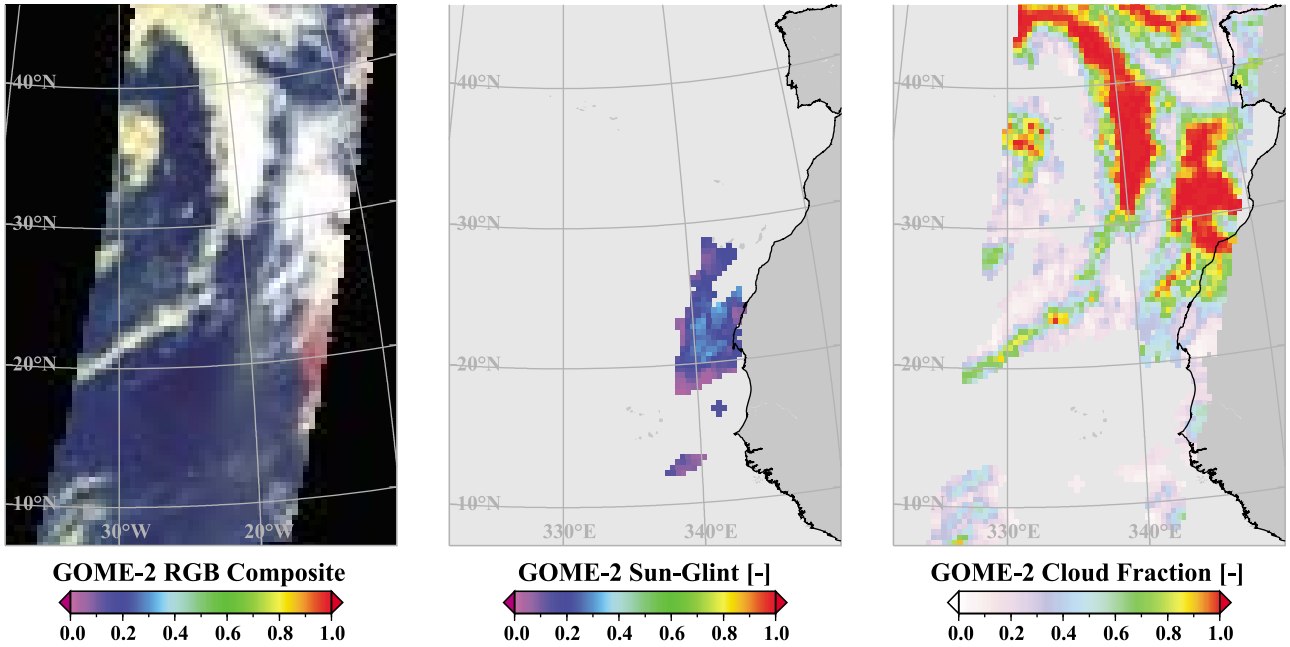

Figure 1. (left) True color composite of the GOME-2 broadband polarization measurements west of Africa (0–40°W, 10–50°N) from 19 April 2010 (orbit 18153). The Sun glint enhanced signal is clearly visible around 20°W, 20°N. (middle) Clouds are properly discriminated from Sun glint. (right) The OCRA cloud fraction for this scene.

sensitive to scattering by aerosols present in a given GOME-2 scene, so that both effects are subsumed in the retrieved cloud fractions.

[12] The impact of cloud properties on the GDP 4.0 ozone retrieval is discussed by *Van Roozendael et al.* [2006]; uncertainties on the estimation of the cloud properties may induce total ozone errors larger than 1%. With GOME-2, several improvements have been incorporated in the cloud algorithms. The initial ROCINN algorithm was based on transmittance-only calculations in the oxygen *A* band. Currently, we use ROCINN version 2.0, based on radiative transfer simulations with Rayleigh scattering and polarization. Comparisons with Meteosat Second Generation cloud data show improvements in cloud albedo (differences of 0.07 ± 0.09) and cloud top height (difference of −0.44 ± 1.26 km); see *Loyola et al.* [2010] for more details.

[13] An important upgrade for GOME-2 is the ability to distinguish clouds in measurements affected by ocean surface Sun glint, a phenomenon that is very common at the edges of the GOME-2 swath. The backscattered radiation under Sun glint conditions may be strongly enhanced, especially at low wind speed (high specular reflection). The resulting signal enhancement is similar to that generated by clouds (Figure 1, left). OCRA correctly discriminates clouds (Figure 1, right) in the region affected by Sun glint (Figure 1, middle) by analyzing the broadband polarization measurements (D. Loyola and W. Zimmer, Cloud properties derived from three years of GOME-2 measurements, manuscript in preparation, 2011).

2.2. Ozone Intracloud Correction

[14] GDP 4.0 uses the "clouds as reflecting boundaries" (CRB) model, where clouds are treated as Lambertian Equivalent Reflectors (some authors name this cloud model "mixed LER" or "Partial Cloud Model" [*Liu et al.*, 2004]). The CRB model assumes that ozone measured by the satellite is confined to the atmosphere above cloud top; the ozone below cloud top is estimated by integrating a suitable climatological ozone profile from cloud top height to the surface. Traditionally, intracloud ozone is not properly handled in retrievals based on the CRB model. Optical path enhancement in clouds is partially taken into account by the cloud properties retrieved with the ROCINN algorithm (based also on the CRB model) and the corresponding changes in oxygen absorption. In reality, clouds are not opaque Lambertian surfaces and light paths penetrate well inside the clouds, especially in case of thin or moderately thick clouds. Satellite measurements are sensitive to intracloud ozone, and neglecting this effect in the retrieval may give rise to significant error in the simulated backscatter signal, thereby inducing appreciable ozone total column errors [*Liu et al.*, 2004].

[15] The ozone ghost column G in equation (1) is obtained by integrating the a priori ozone profile (TOMS v8 climatology in GDP 4.x) from cloud top to the surface. However, this ghost column is actually the difference between the true ozone column under the cloud and the intracloud ozone column, and thus the retrieval will overestimate the total atmospheric column. *Liu et al.* [2004] estimate an ozone retrieval error of more than 17 Dobson Unit (DU) due to the intracloud ozone absorption enhancement of an optically thick water cloud spanning 2–12 km.

[16] GDP 4.4 uses a straightforward correction to the CRB, with clouds treated as semitransparent Lambertian surfaces. The intracloud ozone column V_{ic} is characterized empirically using the formula $V_{ic} = V_{bc}(1 - c_a)\cos(\theta)$, where V_{bc} is the climatological ozone column below cloud top, c_a the cloud albedo and θ the solar zenith angle (SZA).

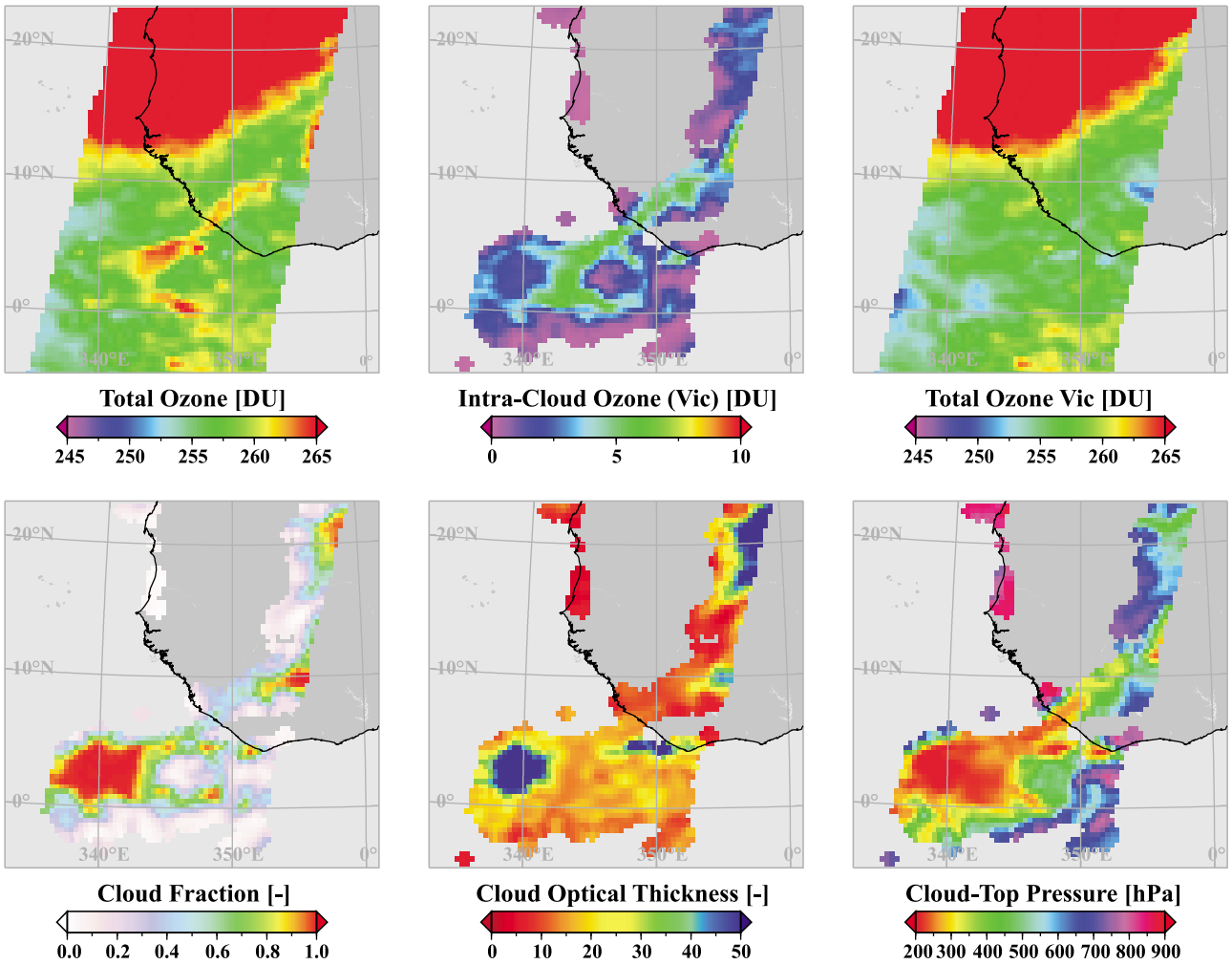

Figure 2. Total ozone retrieval (top left) without and (top right) with intracloud correction for GOME-2 measurements over the equatorial mid-Atlantic region (0–30°W, 5°S–25°N) from 1 April 2007 (orbit 2326). (top middle) The intracloud correction. The corresponding GOME-2 derived cloud properties: (bottom left) cloud fraction, (bottom middle) cloud optical thickness (COT), and (bottom right) cloud top pressure (CTP). The intracloud correction (Figure 2, top middle) is larger for high optical thin clouds (CTP and COT in red).

A simple linear dependency is assumed in this formula; the intracloud ozone is larger for optically thin clouds (smaller cloud albedo, greater photon penetration) and smaller for high SZA (long photon path).

[17] A more accurate ghost column G can be then calculated according to:

$$G = V_{bc} - V_{ic} = V_{bc}(1 + c_a \cos(\theta) - \cos(\theta)) \qquad (2)$$

For optically thin clouds, equation (2) will result in smaller ghost columns which in turn will avoid overestimation of the total ozone. The ghost column correction is larger in equatorial regions where solar zenith angles are smaller.

[18] In tropical regions, the intracloud correction is important in the presence of deep convective clouds. This is seen in Figure 2, which shows intracloud corrections comparing adjacent cloudy and cloud-free ground pixels in the tropical region around 0–10°N 5–20°W with optically thin clouds located at high altitudes. The ozone total column overestimation for cloudy pixels without the intracloud correction is evident, despite the fact that the effective cloud top height derived from oxygen A band measurements is located well inside the cloud [*Vasilkov et al.*, 2008]; the associated ghost column is therefore relatively small. With the intracloud correction, total ozone values are almost the same for cloud-contaminated and clear-sky pixels (Figure 2, right). The smoothly distributed generally low levels of ozone in tropical regions are attributed to vertical injection of ozone poor oceanic boundary layer air followed by convective outflow [*Ziemke et al.*, 2009].

2.3. Ozone Retrieval Over Snow and Ice Conditions

[19] Over snow and ice conditions, it is virtually impossible to distinguish clouds from the ground in the GOME-2 measurements. Over such bright surfaces, the ROCINN algorithm is configured to retrieve effective cloud top height and albedo values for the underlying scene, by fixing the cloud fraction to 1.0. AMFs are then computed with these

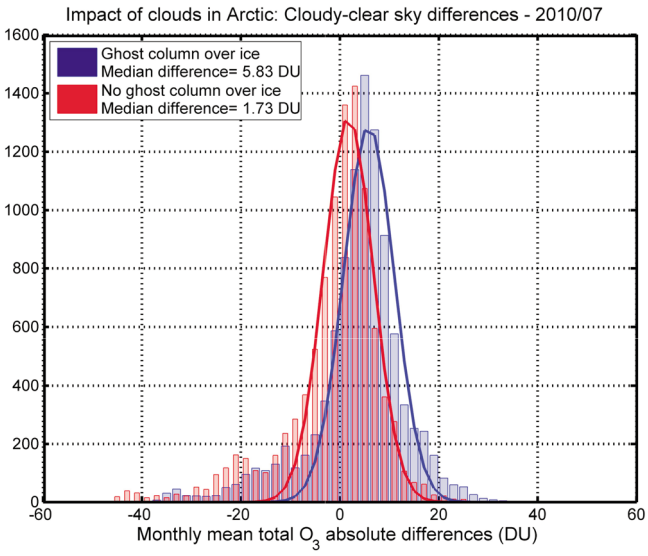

Figure 3. Histograms of the absolute differences between colocated monthly mean total ozone columns considering only cloudy or clear sky pixels treated in the snow/ice mode in the Arctic during July 2010. The blue and red distributions differ on the basis of whether or not a ghost column was added for the cloudy pixels. The Gaussian curves have been fitted to the distributions with their center fixed at the median difference. The red distribution center (no ghost column) is closer to 0.

effective quantities. The ghost column correction is not applied in this special mode. Indeed, the sensitivity to ozone absorption below the cloud over bright surfaces is enhanced compared to that over dark surfaces due to multiple reflections of the radiation between the bright surface and the bottom of the cloud [*Vasilkov et al.*, 2010]. Figure 3 shows the distribution of the absolute differences between the monthly mean total columns considering only clear or cloudy pixels covered by snow/ice in the Arctic for July 2010. A pixel is considered as cloudy when the ROCINN effective cloud top pressure differs from the surface pressure by more than 50 hPa. In general, cloudy scene measurements tend to be larger than clear sky measurements if a ghost column is added in the snow/ice mode, while the distribution of the differences has smaller scatter without this ghost column correction.

[20] Figure 4 shows the differences in the O_3 fields retrieved by adding and omitting ghost O_3 columns. Overall, a decrease of the ozone columns is observed mainly due to the removing of the ghost column correction. Nevertheless, the use of the effective parameters may lead to an increase of the columns in some specific conditions (e.g., the weak tropospheric ozone content and the important surface altitude in Antarctica make the impact of the ghost column small).

2.4. Radiative Transfer Model Simulations With LIDORT 3.3

[21] The role of LIDORT in the GDP 4.0 algorithm for GOME was discussed in detail in [*Van Roozendael et al.*, 2006], and here we confine our attention to an important GOME-2 modification. LIDORT is a plane-parallel multiple-scattering discrete ordinate code that includes a pseudo-spherical approximation, in which solar beam attenuation (before scattering) is treated for a spherically curved atmospheric medium. With its large swath (1920 km), it is necessary with GOME-2 to deal with spherical geometry more accurately in the radiative transfer (RT) calculations. To this end, LIDORT Version 3.3 has an additional sphericity correction, in which the solar and viewing angles change along the line of sight according to the Earth's curvature. Starting at the surface, the RT equation is integrated layer by layer along this path to top of the atmosphere (TOA). Single scatter source terms are computed accurately for each layer according to the local geometry, while layer multiple-scatter (MS) source terms are generated from LIDORT for the solar and viewing geometry at the bottom of the atmosphere (BOA). For details of this RT enhancement, see *Spurr* [2008].

[22] For nominal GOME (swath 960 km) and SCIAMACHY (swath 1000 km) measurements, the maximum scan angle is ~31° at the satellite. In this case, the radiance error induced by omitting the line-of-sight sphericity correction is generally at the 1% level, an acceptable level of uncertainty for the total ozone retrieval itself. However, for GOME-2, the maximum scan angle is ~62° at the satellite, and radiance errors can be as large as 6%–8% at swath edges if the outgoing correction is neglected [*Caudill et al.*, 1997; *Rozanov et al.*, 2000]. Although it is possible to compute the MS contributions at each step along the line of sight, this is computationally expensive (multiple calls to LIDORT), and it was shown by [*Spurr*, 2003; *de Beek et al.*, 2004] that a single call to LIDORT for the MS terms based on the BOA geometry provides sufficient accuracy.

2.5. Correction for Scan Angle Dependency

[23] For all retrievals so far, GOME-2 ozone columns have shown a slight but noticeable instrument scan angle dependency. This has been attributed provisionally to as-yet unknown errors in Level 1b calibration; this is still under investigation. There is a bias of about 1.5%–2% between ozone columns for west and east ground pixels (west higher than east) [*Balis et al.*, 2009; *Antón et al.*, 2009]. This bias is not just a function of the scattering angle, but it also depends on the latitude and solar zenith angle, and it varies from month to month.

[24] With GDP 4.4, we have introduced an empirical correction for the scan angle dependency to remove this bias in the ozone columns. The correction is self-consistent: two full years of GOME-2 data (2007 and 2008) were used to calculate total ozone latitudinal monthly means for every forward scan angle position. Latitudinal mean columns at four west scan angle positions are then selected as reference values to normalize all measurements because west scan measurements agree better with the ground-based measurements. Finally, a polynomial is fitted to the normalized measurements in order to remove outliers and obtain a smoother correction function.

[25] The correction factors are classified according to scan angle, latitude and month of the year. Figure 5 shows correction factors for January and July; the scans used as reference for the correction are marked with the blue arrow. This correction is being applied to all the 24 forward scan pixels. Validation with ground-based data (see Figure 11)

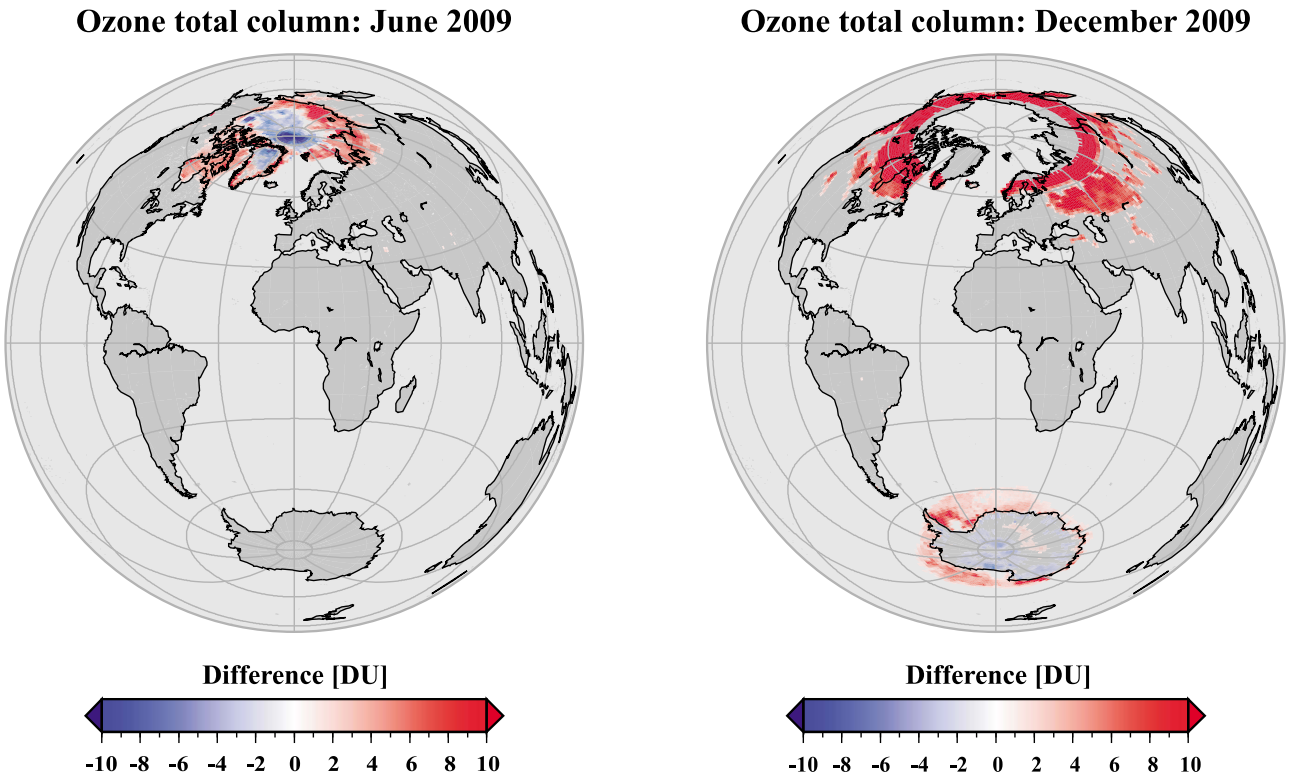

Figure 4. Mean total ozone differences between retrievals without and with snow/ice mode activated for GOME-2 measurements from (left) June 2009 and (right) December 2009. The snow/ice mode results in an overall reduction of the ozone columns in polar regions, leading to improved agreement with the ground-based correlative data sets.

shows that this correction almost completely eliminates the scan angle dependency on GOME-2 total ozone.

3. Ground-Based Validation

3.1. Brewer and Dobson Ozone Total Column Measurements

[26] Ground-based total ozone column measurements contributing to the World Meteorological Organization (WMO)–Global Atmosphere Watch (GAW) network are routinely deposited at the World Ozone and Ultraviolet Radiation Data Centre (WOUDC) in Toronto, Canada (http://www.woudc.org). The WOUDC archive contains total ozone column data mainly from Dobson and Brewer UV spectrophotometers, from the early 1950s onward. The spatial and temporal coverage offered by the archived Dobson and Brewer data records, especially during the last twenty years, provide a wide geographical range for validation of satellite sensors. However, better coverage is achieved over land with respect to sea and over the Northern Hemisphere compared to the Southern Hemisphere. Ground-based Dobson and Brewer spectrophotometers can potentially maintain a 1% level of precision over long time intervals [*Fioletov et al.*, 2005]. In this paper we used archived data from the same stations selected for earlier satellite ozone validation studies [e.g., *Balis et al.*, 2007b].

[27] *Van Roozendael et al.* [1998] have shown that Dobson and Brewer ozone column data agree to within 1% when the major sources of discrepancy are properly accounted for. The standard retrieval from Dobson neglects the temperature dependence of the ozone absorption cross sections, and this could account for a seasonal variation in the error of 0.9% in the middle latitudes and 1.7% in the Arctic. Brewer measurements are also affected by a similar temperature dependence, although it is smaller in amplitude. Small differences between collocated Dobson and Brewer measurements, within 0.6%, are introduced due to the use of different wavelengths and temperature dependencies for the ozone absorption coefficients [*Staehelin et al.*, 2003]. *Fioletov et al.* [2008] compared the Dobson and Brewer data archived in WOUDC to satellite total ozone measurements from TOMS (Nimbus 7, Meteor 3, and Earth Probe), OMI/Aura and GOME/ERS-2 instruments. It was shown that, for the ground stations considered and for 90% of all cases, Dobson and Brewer sites demonstrated 5 year mean differences with satellites to be within ±3% for DS observations.

3.2. Validation Results and Discussion

[28] This validation study is based on a statistical analysis of GOME-2 and ground-based ozone data, performed with respect to time and to various measurement and retrieval parameters. 59 Dobson and 40 Brewer instruments were selected for the validation analysis [*Balis et al.*, 2009]. Data obtained at individual stations are binned in classes of latitude, SZA, pixel scan number, etc. and these binned results are then examined to reveal possible issues and particularities with the satellite data. In Figure 6 (left) the relative difference between GOME-2 and ground-based total ozone

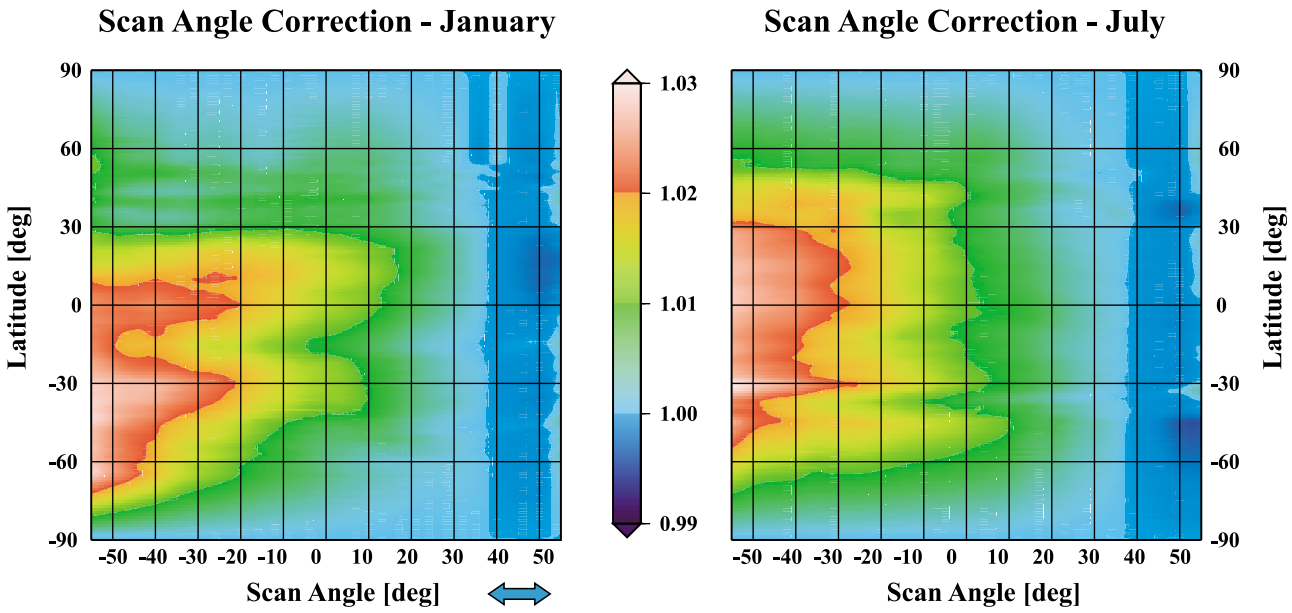

Figure 5. Corrections for scan angle dependency in the total ozone product, plotted as a function of latitude for (left) January and (right) July. Largest correction factors (red) correspond to east pixels, with smaller correction ratios (green) for pixels around the nadir and almost no correction (blue) for west pixels. The blue arrow marks the region used as reference for the scan angle correction.

measurements is presented as a function of latitude. Brewer comparisons are shown in red, Dobson in blue. Data is sparse in the tropical regions for both types of instrument, and nonexistent for the Southern Hemisphere for the Brewers. The mean difference and standard deviation between the GOME-2 and Dobson measurements is −0.28 ± 0.70% and −1.22 ± 0.67% for the Brewer measurements, i.e., within the target of 1% maximum bias and precision.

[29] Figure 6 (right) shows the relative difference between GOME-2 and ground-based measurements as a function of SZA. For low SZAs, GOME-2 underestimates total ozone by −1.5%, whereas for SZA > 65° we see an overestimation of around 1.5% with respect to the Dobsons, but almost no difference with respect to the Brewers. Here it should be noted that Brewer measurements are limited to the Northern Hemisphere and that for large SZAs, the systematic error of the ground-based measurements increases as well. Examining the total ozone column dependency, we found no dependency with the Brewers for total ozone columns greater than 250 DU, as shown in Figure 7 (right); below that value, there is only a single bin with very few common measurements. For the Dobsons no dependency for columns greater than 180 DU was found (Figure 7, left); however, a very high variability was apparent in the 1 σ error bar distribution. It was found that for all months of the year, a change from underestimation to overestimation occurs around 60° in SZA, being most pronounced in August and September at the return of sunlight for the Southern Hemisphere.

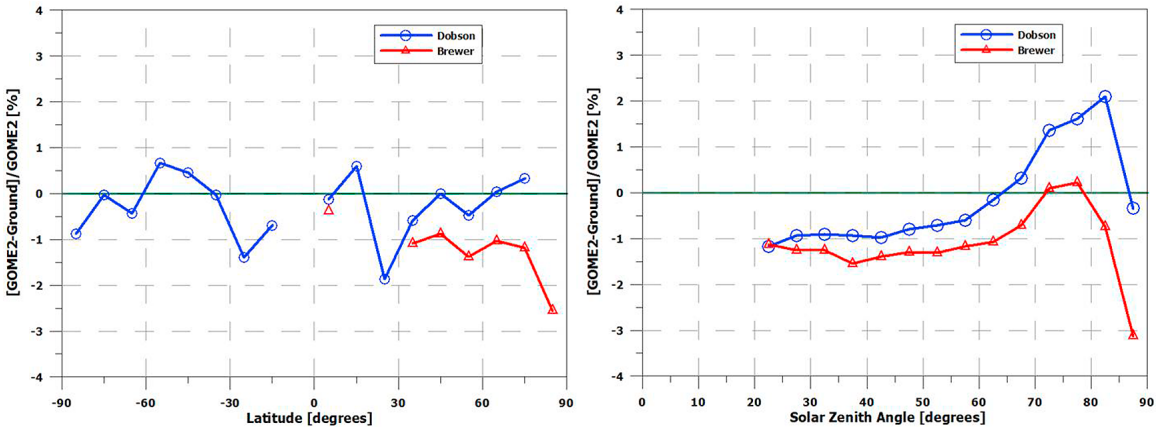

Figure 6. (left) Latitude dependence and (right) solar zenith angle dependence of the relative difference between GOME-2 and Brewer total ozone measurements (red diamonds) and Dobson total ozone measurements (blue circles).

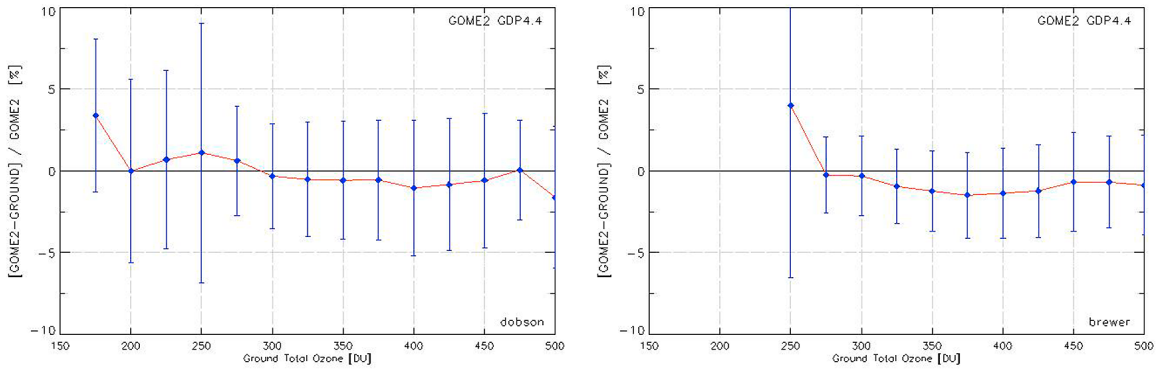

Figure 7. Relative difference between GOME-2 and (left) Dobson total ozone measurements and (right) Brewer total ozone measurements as a function of the ground total ozone column.

[30] The monthly mean hemispheric time series of the differences between GOME-2 and ground-based total ozone differences are depicted in Figure 8. The total ozone seasonal variability is evident, with lows in summer and highs in winter. A small drift in the time series can be observed from August–September 2008 onward, where both comparison curves seem to have shifted upward toward the zero line. In the Southern Hemisphere, this effect cannot be discerned so clearly. This drift could be linked in part to changes in the GOME-2 PMD settings from March 2008, and/or changes in the version of Level 1b data used thereafter.

[31] A contour representation of the monthly mean time series as a function of latitude, as shown in Figure 9, reveals the aforementioned effect more clearly. For example, northward of 30°N, the differences start at −2.5% and gradually rise to 0.5%. For the equatorial regions a small drift in time can be observed. In the Southern Hemisphere, there is a paucity of ground-based data and the situation is less clear. From Figure 9, the drift is also seen to be latitude dependent, indicating quite possibly that both calibration and algorithm issues are at work, such as the effects of the interannual stratospheric temperature variability, which are currently being examined in order to clarify our understanding of these drift patterns. A similar pattern emerges in the validation of GOME and SCIAMACHY observations with the same set of ground-based measurements and the same time period of 2007 to 2009; this is discussed in detail in the latest validation report [*Balis et al.*, 2009] and a forthcoming paper where the GOME2 reprocessed database is validated not only against the ground-based measurements but also against the other satellite estimations.

[32] A seasonal contour plot of the relative differences between GOME-2 and Dobson ozone total columns is shown in Figure 10. GOME-2 overestimates ozone slightly for most of the Southern Hemisphere in all seasons apart from the summer months of January and December. This underestimation of −1% to −2% southward of 60°S is reversed for the winter months of July and August to a ~2% overestimation due to ground-based data paucity and high SZA values. In the Northern Hemisphere, GOME-2 slightly underestimates (−1%) around 20°N for all months, whereas at higher midlatitudes around 50°N it overestimates for the winter months (+1%) and underestimates (−1%) in summer. This picture is consistent with the GOME/ERS-2 findings of *Balis et al.* [2007b].

[33] The empirical correction for the east-west pixel dependency introduced in GDP 4.4 has already been discussed in detail in section 2.5. It is shown below how the

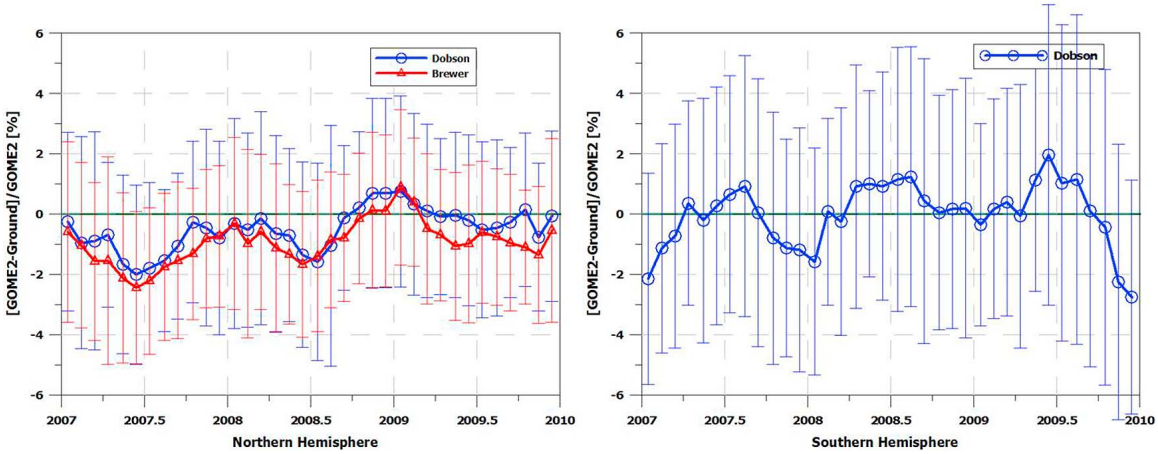

Figure 8. Time series of GOME-2 total ozone comparisons with ground-based data for (left) the Northern Hemisphere and (right) the Southern Hemisphere.

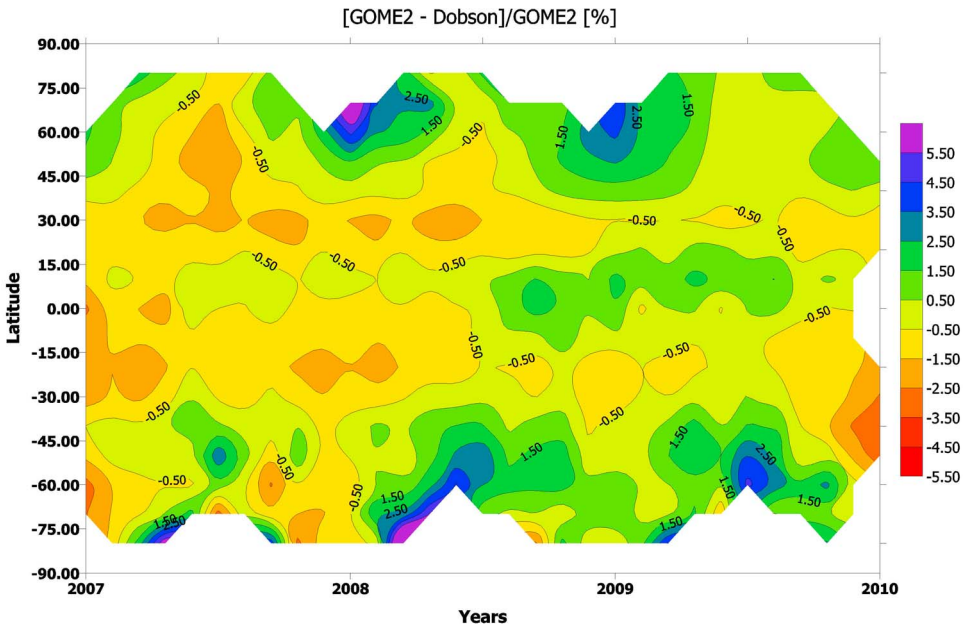

Figure 9. Monthly mean difference between the Dobson and GOME-2 total ozone measurements as a function of latitude and time.

east-west scan angle dependency observed with earlier GOME-2 ozone results is greatly reduced in the reprocessed ozone data used in this work. In Figure 11 the subpixel scan dependence is shown for the nominal (Figure 11, right) and the reprocessed (Figure 11, left) GOME-2 data sets. The forward part of the GOME-2 scan runs from pixel numbers 0 to 24, with east scans from 0 to 11, and west ones between 12 and 24. Three curves are shown, blue for tropical stations (within ±30° latitude), green for midlatitude stations (greater than ±30° latitude), and red diamonds for all stations including polar regions. For the reprocessed GOME-2 GDP 4.4 data set, the east-west dependence is almost eliminated

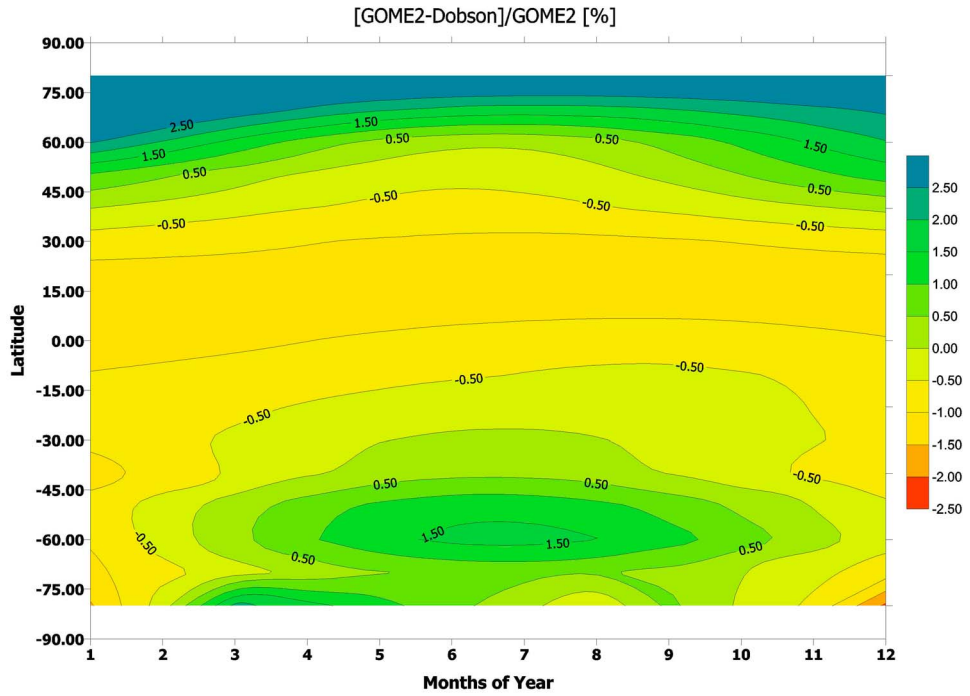

Figure 10. Seasonal dependence of the differences between GOME-2 and Dobson total ozone as a function of latitude.

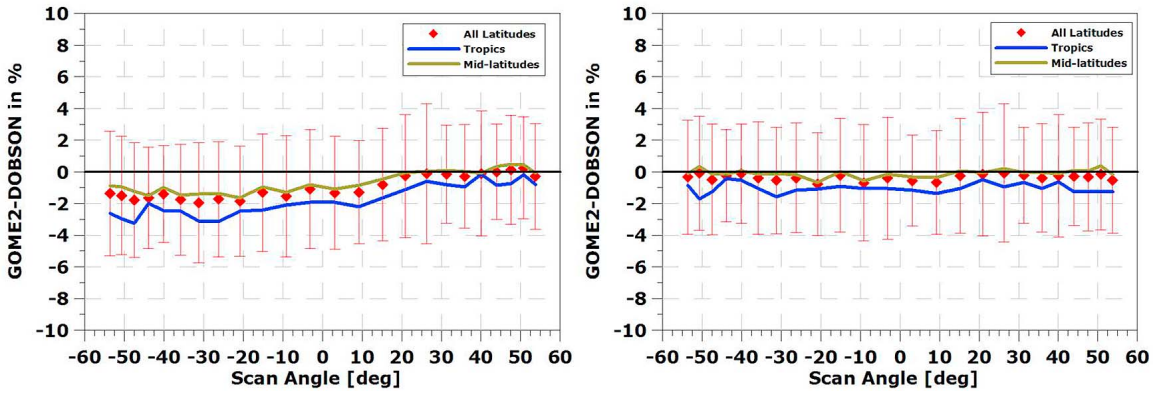

Figure 11. Dependence of the differences between GOME-2 and Dobson total ozone on the GOME-2 scan position (forward scan only). (left) The nominal GDP 4.2 data set and (right) the reprocessed GDP 4.4 data set.

for the forward scans shown here, with a mean below the 1% target difference.

4. Summary and Conclusions

[34] The GOME Data Processor (GDP) version 4.4 retrieval algorithm for GOME-2 total ozone was described. Several algorithm improvements were introduced in GDP 4.4 compared to previous versions such as the correction for intracloud ozone, the improved cloud retrieval algorithms including the discrimination of Sun glint effects, the enhanced treatment for snow and ice conditions, the accurate radiative transfer modeling for large viewing angle conditions and the empirical correction to eliminate scan angle dependency caused by an unknown bias, possibly in the Level 1b radiances however still under investigation. The GDP 4.4 algorithm is shown to be robust in performance and more than capable of real-time data turnover in operational execution.

[35] We have also presented the first global validation results for three years (2007–2009) of GOME-2/MetOp-A total ozone measurements, using Brewer and Dobson ground-based measurements. At middle latitudes, the reprocessed GOME-2 GDP 4.4 data set underestimates ground-based ozone in the Northern Hemisphere, and overestimates ozone in the Southern Hemisphere by around 0.5%. At northern high latitudes, GOME-2 has almost no offset relative to Dobson readings, while at southern high latitudes, GOME-2 underestimates by less than 1%. In the tropics, the GOME-2 underestimation is on average 0 to 2% compared to Dobson measurements. GOME-2 Brewer comparisons over the Northern Hemisphere are consistent with the GOME-2 versus Dobson comparisons and show an underestimation of 1%, which tends to be slightly higher (1%–2%) over the Arctic. A small drift with time has been observed in the reprocessed GOME-2 ozone data. This drift is probably associated with changes in the GOME-2 PMD settings from March 2008 and/or changes in the version of Level 1b data used afterward. This is currently under investigation. An empirical correction introduced in GDP 4.4 removed the scan angle dependency in the GOME-2 reprocessed data. The forward scan west-east bias of more than +1.5% in the previous GDP 4.2 data has been largely eliminated in the reprocessed record.

[36] GOME-2 total ozone products have been generated operationally since March 2007 at the O3M-SAF processing facility in DLR. Near-real-time (i.e., 2 h after sensing), off-line and reprocessed products are freely available. GOME-2 total column products are broadcasted via EUMETCast and WMO/GTS. GOME-2 Level 2 total column and cloud products are additionally available online at ftp://atmos.caf.dlr.de. GOME-2 total ozone products can be ordered at the Help Desk of the O3M-SAF hosted by the Finnish Meteorological Institute (FMI) at o3msaf@fmi.fi. The GOME-2 total column Algorithm Theoretical Basis Document [*Valks et al.*, 2010], Product User Manual, Validation Reports as well as quick look images and links to related services are all available from following DLR web page: http://atmos.caf.dlr.de/gome2. The Laboratory of Atmospheric Physics (LAP) at Aristotle University of Thessaloniki, in collaboration with the Hellenic National Meteorological Service, has developed a total ozone validation facility for GOME-2 data, which can be found at http://lap.physics.auth.gr/eumetsat/totalozone. GOME-2/MetOp-A total ozone obtained with GDP 4.4 continues the GOME and SCIAMACHY time series started in 1995. The GOME-type long-term total ozone data record [*Loyola et al.*, 2009] that will cover a time period of at least 25 years, has reached a high accuracy and stability and is essential for monitoring the expected recovery of the ozone layer resulting from measures adopted as a result of the Montreal protocol and its amendments.

[37] **Acknowledgments.** Development of the GOME-2 total ozone products and their validation has been funded by the O3M-SAF project with EUMETSAT and national contributions. We would like to thank colleagues J. Jaeger, K. H. Seitz, B. Huber, and T. Ruppert who are responsible for day-to-day operations of the O3M-SAF facility at DLR. We thank EUMETSAT for the ground segment interfacing work with the O3M-SAF systems and for the provision of GOME-2 Level 1 products. Ground-based data used in this work were taken from the World Ozone and Ultraviolet Data Centre (WOUDC, http://www.woudc.org).

References

Antón, M., D. Loyola, M. López, J. M. Vilaplana, M. Bañón, W. Zimmer, and A. Serrano (2009), Comparison of GOME-2/MetOp total ozone data with Brewer spectroradiometer data over the Iberian Peninsula, *Ann. Geophys.*, *27*, 1377–1386, doi:10.5194/angeo-27-1377-2009.

Balis, D., M. Kroon, M. E. Koukouli, E. J. Brinksma, G. Labow, J. P. Veefkind, and R. D. McPeters (2007a), Validation of Ozone Monitoring Instrument total ozone column measurements using Brewer and Dobson spectrophotometer ground-based observations, *J. Geophys. Res.*, *112*, D24S46, doi:10.1029/2007JD008796.

Balis, D., et al. (2007b), Ten years of GOME/ERS2 total ozone data—The new GOME data processor (GDP) version 4: 2. Ground-based validation and comparisons with TOMS V7/V8, *J. Geophys. Res.*, *112*, D07307, doi:10.1029/2005JD006376.

Balis, D., M. Koukouli, D. Loyola, P. Valks, and N. Hao (2009), O3MSAF validation report, *Rep. SAF/O3M/AUTH/GOME-2VAL/RP/03*, Eur. Organ. for the Exploit. of Meteorol. Satell., Darmstadt, Germany, Nov. (Available at http://atmos.caf.dlr.de/gome2/docs/AUTH_GOME-2_O3_VAL.pdf.)

Bhartia, P. K., et al. (2002), *OMI Algorithm Theoretical Basis Document*, vol. II, *OMI Ozone Products*, NASA Goddard Space Flight Cent., Greenbelt, Md., Aug. (Available at http://eospso.gsfc.nasa.gov/eos_homepage/for_scientists/atbd/docs/OMI/ATBD-OMI-02.pdf.)

Bovensmann, H., et al. (1999), SCIAMACHY: Mission objectives and measurement modes, *J. Atmos. Sci.*, *56*(2), 127–150, doi:10.1175/1520-0469(1999)056<0127:SMOAMM>2.0.CO;2.

Burrows, J. P., et al. (1999), The global ozone monitoring experiment (GOME): Mission concept and first scientific results, *J. Atmos. Sci.*, *56*, 151–175, doi:10.1175/1520-0469(1999)056<0151:TGOMEG>2.0.CO;2.

Caudill, T. R., D. E. Flittner, B. M. Herman, O. Torres, and R. D. McPeters (1997), Evaluation of the pseudo-spherical approximation for backscattered ultraviolet radiances and ozone retrieval, *J. Geophys. Res.*, *102*, 3881–3890, doi:10.1029/96JD03266.

de Beek, R., M. Weber, V. V. Rozanov, A. Rozanov, A. Richter, and J. P. Burrows (2004), Trace gas column retrieval—An error study for GOME-2, *Adv. Space Res.*, *34*, 727–733, doi:10.1016/j.asr.2003.06.042.

Fioletov, V. E., J. B. Kerr, C. T. McElroy, D. I. Wardle, V. Savastiouk, and T. S. Grajnar (2005), The Brewer reference triad, *Geophys. Res. Lett.*, *32*, L20805, doi:10.1029/2005GL024244.

Fioletov, V. E., et al. (2008), Performance of the ground-based total ozone network assessed using satellite data, *J. Geophys. Res.*, *113*, D14313, doi:10.1029/2008JD009809.

Heinen, T., S. Kiemle, B. Buckl, E. Mikusch, and D. Loyola (2009), The geospatial service infrastructure for DLR's National Remote Sensing Data Library, *IEEE J. Sel. Top. Appl. Earth Obs. Remote Sens.*, *2*, 260–269, doi:10.1109/JSTARS.2009.2037598.

Lerot, C., et al. (2009), Six years of total ozone column measurements from SCIAMACHY nadir observations, *Atmos. Meas. Tech.*, *2*, 87–98, doi:10.5194/amt-2-87-2009.

Liu, X., M. Newchurch, R. Loughman, and P. K. Bhartia (2004), Errors resulting from assuming opaque Lambertian clouds in TOMS ozone retrieval, *J. Quant. Spectrosc. Radiat. Transfer*, *85*, 337–365, doi:10.1016/S0022-4073(03)00231-0.

Loyola, D., W. Thomas, Y. Livschitz, T. Ruppert, P. Albert, and R. Hollmann (2007), Cloud properties derived from GOME/ERS-2 backscatter data for trace gas retrieval, *IEEE Trans. Geosci. Remote Sens.*, *45*(9), 2747–2758, doi:10.1109/TGRS.2007.901043.

Loyola, D., M. Coldewey-Egbers, M. Dameris, H. Garny, A. Stenke, M. Van Roozendael, C. Lerot, D. Balis, and M. Koukouli (2009), Global long-term monitoring of the ozone layer—A prerequisite for predictions, *Int. J. Remote Sens.*, *30*(15), 4295–4318, doi:10.1080/01431160902825016.

Loyola, D., W. Thomas, R. Spurr, and B. Mayer (2010), Global patterns in daytime cloud properties derived from GOME backscatter UV-VIS measurements, *Int. J. Remote Sens.*, *31*, 4295–4318.

McPeters, R. D., G. J. Labow, and J. A. Logan (2007), Ozone climatological profiles for satellite retrieval algorithms, *J. Geophys. Res.*, *112*, D05308, doi:10.1029/2005JD006823.

Munro, R., M. Eisinger, C. Anderson, J. Callies, E. Corpaccioli, R. Lang, A. Lefebvre, Y. Livschitz, and A. Perez Albinana (2006), GOME-2 on METOP: From in-orbit verification to routine operations, paper presented at EUMETSAT Meteorological Satellite Conference, Eur. Organ. for the Exploit. of Meteorol. Satell., Helsinki, 12–16 June.

Rozanov, A. V., V. V. Rozanov, and J. P. Burrows (2000), Combined differential-integral approach for the radiation field computation in a spherical shell atmosphere: Nonlimb geometry, *J. Geophys. Res.*, *105*, 22,937–22,942, doi:10.1029/2000JD900378.

Slijkhuis, S., A. von Bargen, W. Thomas, and K. Chance (1999), Calculation of under-sampling correction spectra for DOAS spectral fitting, in *ESAMS'99—European Symposium on Atmospheric Measurements From Space*, *Rep. ESA WPP-161*, pp. 563–569, Eur. Space Agency, Noordwijk, Netherlands.

Spurr, R. J. D. (2003), LIDORT V2PLUS: A comprehensive radiative transfer package for UV/VIS/NIR nadir remote sensing: A general quasi-analytic solution, *Proc. SPIE Int. Soc. Opt. Eng.*, *5235*, 89–100.

Spurr, R. (2008), LIDORT and VLIDORT: Linearized pseudo-spherical scalar and vector discrete ordinate radiative transfer models for use in remote sensing retrieval problems, in *Light Scattering Reviews*, vol. 3, edited by A. Kokhanovsky, pp. 229–275, doi:10.1007/978-3-540-48546-9_7, Springer, Berlin.

Staehelin, J., J. Kerr, R. Evans, and K. Vanicek (2003), Comparison of total ozone measurements of Dobson and Brewer spectrophotometers and recommended transfer functions, *WMO TD 1147*, no. 149, World Meteorol. Organ., Geneva, Switzerland.

Valks, P., D. Loyola, N. Hao, M. Rix, and S. Slijkhuis (2010), Algorithm Theoretical Basis Document for GOME total column products of ozone, NO_2, SO_2, BrO, H_2O, tropospheric NO_2 and cloud properties, *DLR/GOME/ATBD/01*, issue 2, rev. C, Dtsch. Zent. fur Luft und Raumfahrt, Oberpfaffenhofen, Germany. (Available at http://atmos.caf.dlr.de/gome2/docs/DLR_GOME-2_ATBD.pdf.)

Van Roozendael, M., et al. (1998), Validation of ground-based UV-visible measurements of total ozone by comparison with Dobson and Brewer spectrophotometers, *J. Atmos. Chem.*, *29*, 55–83, doi:10.1023/A:1005815902581.

Van Roozendael, M., D. Loyola, R. Spurr, D. Balis, J.-C. Lambert, Y. Livschitz, P. Valks, T. Ruppert, P. Kenter, and C. Fayt (2006), Reprocessing the 10-year GOME/ERS-2 total ozone record for trend analysis: The new GOME data processor version 4.0, algorithm description, *J. Geophys. Res.*, *111*, D14311, doi:10.1029/2005JD006375.

Vasilkov, A., J. Joiner, R. Spurr, P. K. Bhartia, P. Levelt, and G. Stephens (2008), Evaluation of the OMI cloud pressures derived from rotational Raman scattering by comparisons with other satellite data and radiative transfer simulations, *J. Geophys. Res.*, *113*, D15S19, doi:10.1029/2007JD008689.

Vasilkov, A. P., J. Joiner, D. Haffner, P. K. Bhartia, and R. J. D. Spurr (2010), What do satellite backscatter ultraviolet and visible spectrometers see over snow and ice? A study of clouds and ozone using the A-train, *Atmos. Meas. Tech.*, *3*, 619–629.

Zerefos, C., G. Contopoulos, and G. Skalkeas (Eds.) (2009), *Twenty Years of Ozone Decline: Proceedings of the Symposium for the 20th Anniversary of the Montreal Protocol*, Springer, Dordrecht, Netherlands.

Ziemke, J. R., J. Joiner, S. Chandra, P. K. Bhartia, A. Vasilkov, D. P. Haffner, K. Yang, M. R. Schoeberl, L. Froidevaux, and P. F. Levelt (2009), Ozone mixing ratios inside tropical deep convective clouds from OMI satellite measurements, *Atmos. Chem. Phys.*, *9*, 573–583, doi:10.5194/acp-9-573-2009.

D. S. Balis and M. E. Koukouli, Laboratory of Atmospheric Physics, Aristotle University of Thessaloniki, GR-54124 Thessaloniki, Greece. (mariliza@auth.gr)

N. Hao, S. Kiemle, D. G. Loyola, P. Valks, and W. Zimmer, German Aerospace Center, PO Box 1116, D-82234 Wessling, Germany.

J.-C. Lambert, C. Lerot, and M. Van Roozendael, Belgian Institute for Space Aeronomy, 3, av. Circulaire, B-1180 Brussels, Belgium.

R. J. D. Spurr, RT Solutions, Inc., Cambridge, MA 02138, USA.